Laser and Particle Beams (2013), *31*, 273–288.

doi:10.1017/S0263034613000244

Numerical study of radiative opacity for carbon and aluminum plasmas produced by high power pulsed lasers

MOHAMMAD HOSSEIN MAHDIEH AND SAHAR HOSSEINZADEH
Department of Physics, Iran University of Science and Technology, Narmak, Tehran, Iran
(Received 21 November 2012; Accepted 20 March 2013)

Abstract

In this paper, the opacity of plasma in local thermodynamic equilibrium condition was investigated numerically. The plasma was assumed to be produced by interaction of high power pulse laser with carbon and aluminum. Spectrally resolved opacities under different plasma temperature and density conditions were calculated and radiative absorption due to three absorption mechanisms; inverse bremsstrahlung, photo-ionization, and line absorption in plasmas was studied numerically. The purpose of this study is to calculate the values of absorption for inverse bremsstrahlung and photo-ionization processes for aluminum and carbon plasmas and to compare them for those of cold matter. In this investigation, the influences of density and temperature on plasma absorption were evaluated. The calculation results show that the opacity strength strongly depends on the plasma temperature and density.

Keywords: Laser plasma interaction; Opacity; Plasma; Radiation transport; Radiative absorption

INTRODUCTION

The radiative opacity plays an important role in several research areas such as inertial confinement fusion (Orlov *et al.*, 2011; Kauffman *et al.*, 1994; André *et al.*, 1994), and stellar physics (Rogers & Iglesias, 1994; Rose, 1991). Experimental and theoretical determination of plasma opacity within the X-ray spectral range is also important in some applications such as designing laser produced X-ray sources (Meister *et al.*, 2011; Nishimura *et al.*, 1993; Bastiani *et al.*, 1995; Marzi *et al.*, 2000; Babonneaua *et al.*, 1991; Orlov *et al.*, 2007; Zhang *et al.*, 1996), and plasma diagnostics (Zastrau *et al.*, 2012; Jiao-Long *et al.*, 2003). Due to the wide practical applications of radiative opacity, it has remained a subject of current studies until now and many efforts are being made to develop new models and numerical codes for evaluation of such plasmas (Gil *et al.*, 2013; Orlov *et al.*, 2011; Mínguez Torres *et al.*, 2010; Rozsnyai *et al.*, 2010; Rodriguez *et al.*, 2008; Gupta & Kumar, 1995; Ramis *et al.*, 2009; Godwal *et al.*, 1997; Rickert *et al.*, 1990).

High power pulsed lasers are capable for producing plasma as an intense X-ray radiation source. There are many reports in optimization of laser-plasma X-ray sources using various laser parameters and target materials. In this application, opacity is also a crucial factor in optimization of laser-plasma X-ray sources. For example, cocktail targets (mixture of two or more high-*Z* materials) have been widely proposed for enhancing the X-ray emission (Orzechowsk *et al.*, 1996; Gauthier *et al.*, 1999; Gupta & Godwal, 2001). It was shown that if the high opacity region of one element overlaps with the low opacity region of the other, it is possible to obtain higher Rosseland mean opacity as compared to either of the elements in the mixtures. As a result, higher re-emission and conversion efficiency of laser light to X-ray can be achieved with such mixtures (Orzechowsk *et al.*, 1996; Gauthier *et al.*, 1999; Gupta & Godwal, 2001).

In plasmas diagnostics, some properties such as temperature, density, and different ionization stage distribution can be determined by diagnosis of plasma radiation. However, the plasma radiation is influenced by opacity that leads to non-realistic characterization. Such a problem can be solved by combining the experimental results with those of calculations in which opacity is involved (Nishimura *et al.*, 1993; Bastiani *et al.*, 1995).

Within the last two decades, the opacity of plasmas over a wide range of temperature and density has been studied extensively both experimentally and theoretically (Rose, 1992; Bailey *et al.*, 2009). In most of these studies, local thermodynamic equilibrium (LTE) conditions were assumed for plasmas. However, due to a large number of atomic data, the

Address correspondence and reprint requests to: Mohammad Hossein Mahdieh, Department of Physics, Iran University of Science and Technology, Narmak, Tehran, Iran. E-mail: mahdm@iust.ac.ir

calculation of radiative properties of plasma is a difficult task even for low-Z elements. Such atomic data includes the atomic levels and associated involved transitions, spectral line shapes, oscillator strengths, atomic (and ionic) populations, and photo-ionization cross sections. Therefore, the attempts for accurate calculations of radiative opaque plasma are still in progress. Many efforts are being made to develop new models and numerical codes for evaluation of such plasmas (Gupta & Godwal, 2002; Yongqiang *et al.*, 2009). We have also reported preliminary results for calculation of opacity of carbon and aluminum plasmas (Mahdieh & Hosseinzadeh, 2010). However, the calculations were performed for restricted conditions.

In this paper, we have tried to study the opacity of low-Z plasmas ($Z < 30$) by developing a computer code. In some experiments, it is very important to estimate the variation of X-ray opacity in irradiated target for cold matter (Rossall *et al.*, 2010). Abundant calculation of the radiative opacity characteristics in plasmas (temperature and density dependent) results in better understanding of physical processes in plasma produced by a high-power pulsed laser, and that is an advantage of the presented work. In addition, a comparison between the opacity of the cold matter and its plasma can be of interest for those researchers who measure the opacity of matter in a laser produced plasma experiment. Therefore, in this paper, we focused on studying the opacity of carbon and aluminum plasmas for variety range of densities and temperatures and the results were compared with the results of cold material. Furthermore, a main difference between this work and the others that are already reported in the literature is the use of some databases such as NIST Atomic Spectra Database (Martin *et al.*, 2006) for calculating the opacity. In the present work, the plasma was assumed to be in LTE and frequency dependent opacity was calculated. Atomic structure, levels, energies, oscillator strengths, and other atomic data are also provided by either analytical calculations or available data bases. These data will be referenced in the next sections where appropriate. The calculation results were compared with data from the TOPbase data (Magee *et al.*, 1995) and also with other results such as those from Zeng *et al.* (2001) and Gil *et al.* (2013).

THEORY AND COMPUTATIONAL METHOD

Population Densities of Ions

To obtain the opacity, the population densities of neutral to fully ionized ions of plasma components are required. For plasmas in LTE, the population distributions of different ionization stages are given by the well-known Saha-Boltzmann equation (Cowan, 1981) but modified for ionization potential:

$$\frac{N_{i+1}N_e}{N_i} = 2\left(\frac{2\pi mk_BT}{h^2}\right)^{3/2}\frac{U_{i+1}}{U_i}e^{\frac{-(\phi_i - \Delta\phi_i)/k_BT}{k_BT}}, \quad (1)$$

where N_i is the total population density of ion i, N_e is the number of free electrons per unit volume, ϕ_i is the ionization potential of ion i, $\Delta\phi_i$ is the depression of the ionization limit caused by plasma environment restricting the number of bound states available, h is the Planck constant, k_B is the Boltzmann constant, T is the temperature, m is the electron mass, and U_i is the partition functions for ion i and is given by:

$$U_i = \sum_i g_{il}e^{\frac{-E_{il}}{k_BT}}. \quad (2)$$

Where $g_{il} = 2J + 1$ is the statistical weight of the state l, E_{il} is the energy of level l of ion i above the ground state. In solving the Saha-Boltzmann Eq. (1), calculation of the ionization potential depression (IPD) is needed. We chose the Debye-Huckel model (Heading *et al.*, 1995) to calculate the IPD. In the Debye-Huckel model of the plasma potential, the largest radius of an electron that can still be bound is given by the Debye radius. In this model the IPD is given by:

$$\Delta\phi_i = \frac{ze^2}{4\pi\varepsilon_0}\sqrt{\frac{e^2N_e}{\varepsilon_0 k_BT}}. \quad (3)$$

In the LTE plasma, the population density N_{il} for level l of ion stage is determined by Boltzmann distribution function:

$$N_{il} = g_{il}\left(\frac{N_i}{U_i}\right)e^{\frac{-E_{il}}{k_BT}}. \quad (4)$$

Opacity Modeling

The opacity of the material is mainly due to the absorption of photons through the processes: free-free (ff) absorption (or inverse bremsstrahlung), bound-free (bf) absorption (or photo-ionization), bound-bound (bb) absorption (or line absorption), and photon scattering processes. Hence, the total opacity for a photon at energy hν in plasma at temperature T is given by (Eliezer, 2002):

$$k(h\nu) = \frac{1}{\rho}\left[k_{ff}(h\nu) + k_{bf}(h\nu) + k_{bb}(h\nu)\right] \times (1 - e^{\frac{-h\nu}{k_BT}}) + k_{scatt}(h\nu). \quad (5)$$

Where ρ denotes the density of plasma and v is the frequency of photon. The exponential term represents the correction for stimulated emission. Electron scattering is usually not an important contribution to the total opacity. It dominates only at very high temperatures, where other sources tend to decrease.

There are different theoretical models, such as average atom (AA) (Rozsnyai, 1997), under solved transition arrays (UTA) (Bauche & Bauche-Arnoult, 1996), super transition array (STA) (Faussurier *et al.*, 2001), and detailed level accounting (DLA) (or detailed term accounting DTA)

https://doi.org/10.1017/S0263034613000244 Published online by Cambridge University Press

Table 1. *The ionization potential (IP) in (Moore, 1970) and the calculated ionization potential depression (IPD) for aluminum plasma with the temperature of 20 eV and density of 0.01 g/cm^3*

Ions	IP (eV)	IPD (eV)
Al I	5.98	1.29
Al II	18.82	2.59
Al III	28.44	3.88
Al IV	119.99	5.18
Al V	153.71	6.48
Al VI	190.47	7.77
Al VII	241.43	9.07
Al VIII	284.59	10.37
Al IX	330.21	11.66
Al X	398.57	12.96
Al XI	442.07	14.26
Al XII	2086.00	15.55
Al XIII	2304.10	16.85

(Zeng *et al.*, 2006) that take different analysis on the above process. Up to now DLA has achieved great success in predicting the opacity of low-*Z* plasma.

The early attempts of theoretical models for the calculation of the radiative opacity were based on the statistical methods. The self-consistent AA (Green, 1964), and the UTA (Bauche *et al.*, 1978) are some examples. Since lines of different transition arrays are unresolved, STA (Bar-Shalom *et al.*, 1989) was developed which is based on the statistical method. However, theoretical modeling for the radiative opacity of high temperature plasmas involves to plasma conditions, atomic data, state populations, and also spectral line shapes. The spectral line shapes separately can be involved to some broadening mechanisms, such as natural width, Doppler broadening, auto ionizing resonance, and collisional broadening. The models of DTA and DLA consider these issues. Although, the DTA and DLA models are very complex, since one has to obtain a great number of atomic data and to consider many different physical effects on the atomic data, they are more suitable for obtaining detailed spectrally resolved opacity. To date, DTA and DLA have achieved great success in predicting the opacity of low-*Z* plasmas such as aluminum (Abdallah & Clark, 1991; Iglesias *et al.*, 1994; Zeng *et al.*, 2000). It was shown that an accurate opacity can be obtained by using a DLA model for a wide range of plasmas, which are of great utility in many practical researches (Zeng *et al.*, 2006). Therefore, in this work, the plasma opacity has been calculated by using of DLA model which is described in the following section.

Free-Free Opacity

When a free electron moves in the Coulomb field of an ion the system, it emits radiation, while in the inverse process a photon is absorbed. The inverse bremsstrahlung or ff absorption coefficient is given by the semi-classical Kramer's formula (Zel'dovich & Raizer, 1966).

$$\kappa_{ff}(h\upsilon) = \frac{4}{3}\left[\frac{2\pi}{3m_e k_B T}\right]^{1/2} \times G_{ff}\,\frac{N_e e^6}{hcm\upsilon^3}\sum_i N_i Z_i^2, \qquad (6)$$

where, e is the electron charge, and c is the speed of light. The parameters N_e and N_i are the electron and ion densities,

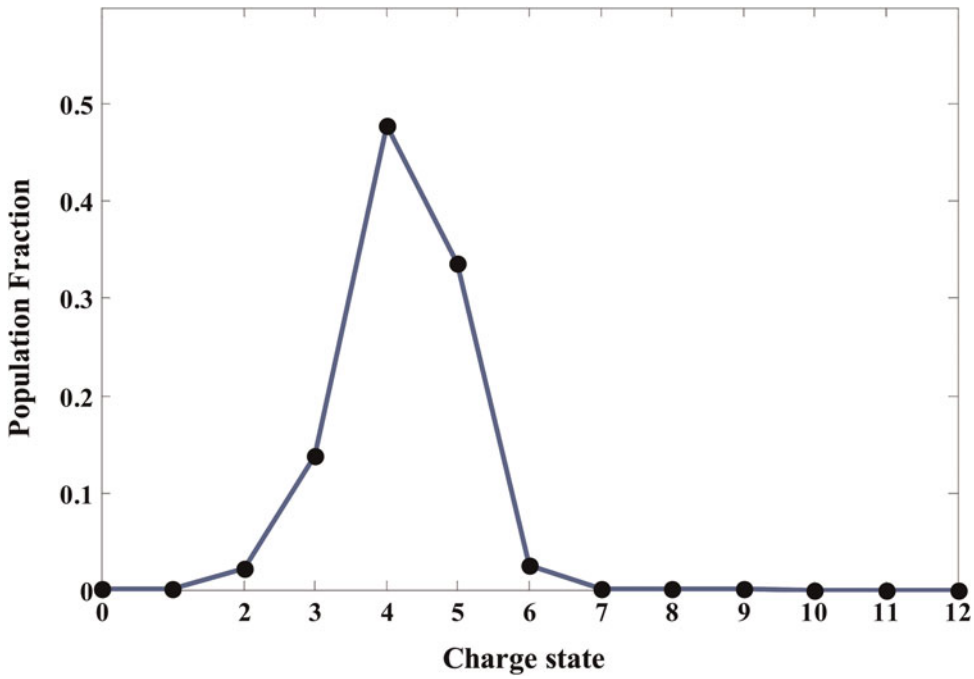

Fig. 1. (Color online) Population fraction versus the charge state for aluminum plasma at temperature 20 eV, and density of 0.01 g/cm^{-3}, respectively.

https://doi.org/10.1017/S0263034613000244 Published online by Cambridge University Press

Table 2. *The atomic data (oscillator strengths f_{ik},energy levels E_i and E_k and statistical weights g) for lower level i to upper level k of Al VI ion from NIST (Martin* et al.*, 2006)*

λ (nm)	f_{ik}	E_i (eV)	E_k(eV)	Lower level			Upper level			g_i	g_k
				configuration	Term	J	configuration	Term	J		
7.4444	8.73e-02	0.00	166.550	2s22p4	3P	2	2s22p3(2D°)4d	3P°	2	5	5
8.5806	3.03e-01	0.4747	144.969	2s22p4	3P	0	2s22p3(2P°)3d	3D°	1	1	3
9.0196	4.27e-01	5.1041	142.564	2s22p4	1D	2	2s22p3(2D°)3d	1F°	3	5	7
10.9284	1.68e-01	10.93	124.389	2s22p4	1S	0	2s22p3(2P°)3s	1P°	1	1	3
11.3629	1.01e-01	40.5199	149.634	2s2p5	3P°	0	2s2p4(4P)3s	3P	1	1	3
22.1535	2.85e-04	0.00	55.9660	2s22p4	3P	2	2s2p5	1P°	1	5	3
24.3766	2.00e-01	5.1041	55.9660	2s22p4	1D	2	2s2p5	1P°	1	5	3
27.5343	8.13e-02	10.937	55.9660	2s22p4	1S	0	2s2p5	1P°	1	1	3
30.7249	3.66e-02	0.00	40.3530	2s22p4	3P	2	2s2p5	3P°	1	5	3
31.0907	1.44e-01	0.4747	40.3530	2s22p4	3P	0	2s2p5	3P°	1	1	3
32.8696	1.51e-01	55.9660	93.6859	2s2p5	1P°	1	2p6	1S	0	3	1
42.146	1.05e-04	10.937	40.3530	2s22p4	1S	0	2s2p5	3P°	1	1	3
107.766	1.03e-01	122.328	133.833	2s22p3(4S°)3p	3P	1	2s22p3(4S°)3d	3D°	1	3	3
108.765	3.27e-01	128.903	140.303	2s22p3(2D°)3p	1F	3	2s22p3(2D°)3d	1G°	4	7	9
132.057	2.31e-01	119.2	128.549	2s22p3(2D°)3s	3D°	3	2s22p3(2D°)3p	3F	4	7	9
135.879	2.68e-01	113.211	122.336	2s22p3(4S°)3s	3S°	1	2s22p3(4S°)3p	3P	2	3	5
135.996	1.61e-01	113.211	122.328	2s22p3(4S°)3s	3S°	1	2s22p3(4S°)3p	3P	1	3	3
140.998	4.74e-02	123.187	131.980	2s22p3(2P°)3s	3P°	0	2s22p3(2P°)3p	3S	1	1	3
141.605	4.94e-02	123.225	131.980	2s22p3(2P°)3s	3P°	2	2s22p3(2P°)3p	3S	1	5	3
142.258	1.46e-01	119.2	127.876	2s22p3(2D°)3s	3D°	3	2s22p3(2D°)3p	3D	3	7	7
143.052	1.14e-01	119.2	127.828	2s22p3(2D°)3s	3D°	2	2s22p3(2D°)3p	3D	2	5	5
143.251	9.79e-02	119.2	127.816	2s22p3(2D°)3s	3D°	1	2s22p3(2D°)3p	3D	1	3	3
144.217	2.31e-01	120.307	128.903	2s22p3(2D°)3s	1D°	2	2s22p3(2D°)3p	1F	3	5	7

respectively. The parameter Z_i is the ionic charge number, and summation is given for all ions. The parameter G_{ff} is the ff Gaunt factor. The Gaunt factor $G_{ff} = 1$ at low temperatures <400 eV or $G_{ff} = 1.4$at temperatures >400 eV (Hutchinson, 2002). Similarly, $G_{ff} = 0$ for photon energy less than the ground state ionization potential, but otherwise $G_{ff} = 1$. In Eq. (5), by summing over all ions present in a plasma, the total ff opacity can be evaluated at a given frequency and temperature.

Bound-Free Opacity

Bound-free absorption occurs when a photon is absorbed by a bound electron, the process is associated with the release of a bound electron around an atom or ion. The bf absorption coefficient can be obtained by:

$$\kappa_{bf}(h\upsilon) = \sum_i N_i \sigma_{ibf}(h\nu), \tag{7}$$

where $\sigma_{ibf}(h\nu)$ is the photo-ionization cross-section per ion *i*. For the present work, all the photo-ionization cross-sections were obtained from the reference (Verner *et al.*, 1996).

Bound-Bound Opacity

In this case, an electron is moved from one bound orbit in an atom or ion to an orbit of higher energy due to the absorption of a photon. The bb opacity for photon at energy *hν* is given by:

$$\kappa_{bb}(h\upsilon) = \sum_i \left(\sum_{ll'} N_{il} \sigma_{ill'}(h\nu) \right), \tag{8}$$

where $\sigma_{ill'}(h\nu)$ is the cross-section for the photo-excitation process from level *l* to *l'* and is given by:

$$\sigma_{ill'}(h\upsilon) = \frac{\pi h e^2}{m_e c} f_{ill'} S(h\nu). \tag{9}$$

The bb cross-section is a function of the oscillator strength $f_{ill'}$, and $S(h\nu)$ denotes the line profile. In this work, Doppler broadening has been taken into account for $S(h\nu)$ (Hutchinson, 2002). By comparing the results of the present work with those of some other available calculations (which will be shown in the following sections), we concluded that the Doppler broadening may be enough to give accurate results for the calculations. However, for more precise calculations, one needs to consider other line profiles such as Stark broadening. In Eq. (7), by summing over all ions, and related level populations the total bb opacity can be evaluated at a given frequency and for given plasma.

The atomic data used in this work (ionization energies, energy levels, statistical weights, and the oscillator strengths) were also taken from the National Institute of Standards and Technology (NIST), they are the most accurate sources and

https://doi.org/10.1017/S0263034613000244 Published online by Cambridge University Press

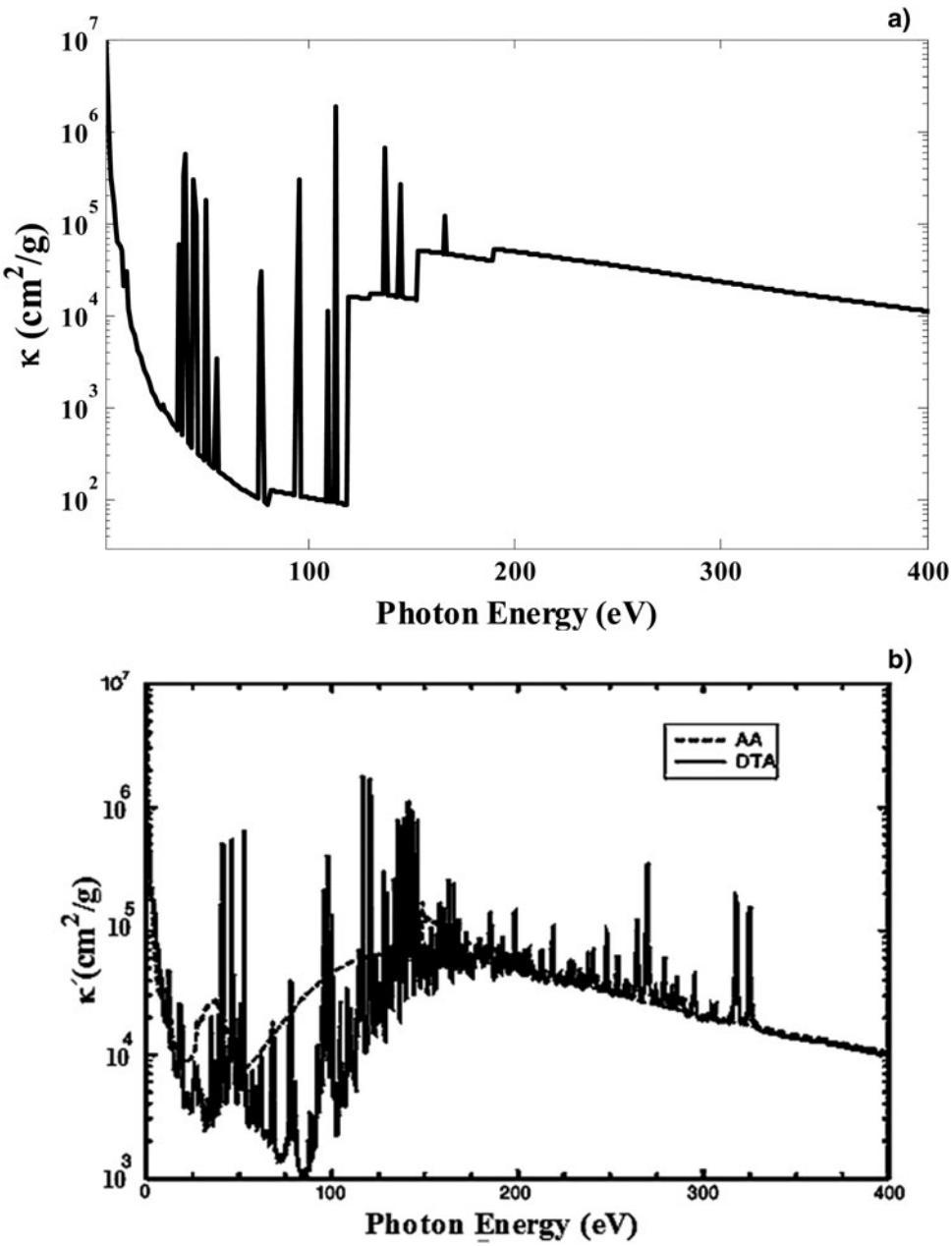

Fig. 2. Frequency-dependent opacity versus incident photon energy for aluminum plasma at temperature 20 eV, and density of 0.01 g/cm^{-3}. (**a**) Present work and (**b**) results reported by (Zeng *et al.*, 2001). The solid line refers to the detailed level accounting calculation and the dashed line to the average atom model (Zeng *et al.*, 2001).

calculations known at present (Martin *et al.*, 2006). These NIST data were produced by combination of experiment and calculations. For example, some energy levels of aluminum (Al I through Al XIII) were critically compiled, mainly from published material on measurements and analyses of the optical spectra but Martin and Zalubas (1979) derived or recalculated the levels for a number of the ions.

CODE VALIDATION

Using the formulae and method discussed in the previous section, a computer code was developed for calculating the radiative opacity under different plasma temperature and density conditions. In order to verify the validation of the code and the computational technique, the code was applied to aluminum plasma with temperature of 20 eV and density of 0.01 g/cm^3, and the radiative opacity was calculated. The radiative opacity of this plasma condition can be given by Rosseland Mean Opacity Tables (Rogers & Iglesias, 1992). The radiative opacity of such plasma condition was also measured experimentally by Winhart *et al.* (1996), and verified numerically by Zeng *et al.* (2001).

By solving the set of nonlinear modified Saha-Boltzmann Eq. (1), the population distribution of aluminum plasma

https://doi.org/10.1017/S0263034613000244 Published online by Cambridge University Press

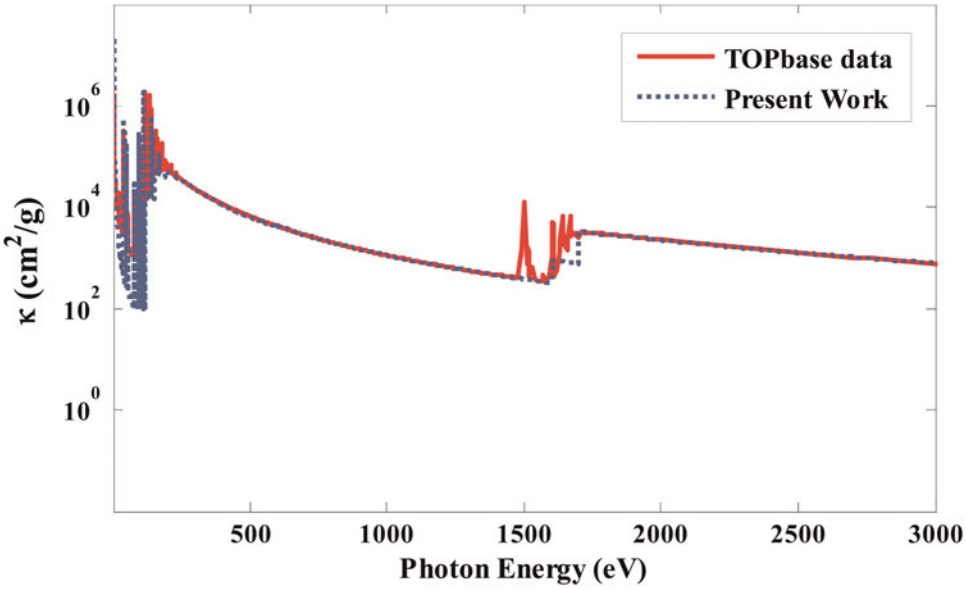

Fig. 3. (Color online) Frequency-dependent opacity versus incident photon energy for 20 eV aluminum plasma at density of 0.01 g/cm^{-3}.

components (including neutrals, partially ionized, and fully ionized ions) were calculated. In these calculations, the total number of charged and neutral particles were assumed to be constant (the total number of particles is the atomic density of the initial neutrals). The ionization potential (IP) in eV (Moore, 1970) and the calculated ionization potential depression (IPD) for different ionization stages for aluminum plasma with the temperature of 20 eV and density of 0.01 g/cm^3 are listed in Table 1. Figure 1 shows the ion population fractions versus the charge state Z_i for aluminum plasma at temperature of 20 eV and density of 0.01 g/cm^3. As Figure 1 shows, in such density and temperature, the most abundant species in the plasma are Al V, Al VI, and Al IV ions with a population of about 50%, 33%, and 14%, respectively.

The calculations show an average ionization degree of 4.2. This value is in good agreement with the result of the OPAL opacity code, which gives 4.3 (Iglesias & Rogers, 1996) and that of Jin *et al.* (2008) who reported a value of 4.2 average ionization degree. Using the ions population fractions data, the opacity was also calculated for the above mentioned aluminum plasma and the results were compared with those reported by Zeng *et al.* (2001) and those in TOPbase data (Magee *et al.*, 1995).

As an example, the atomic data (oscillator strengths f_{ik}, energy levels E_i and E_k and statistical weights g) for lower level i to upper level k of Al VI ion, taken from the NIST (Martin *et al.*, 2006) are listed in Table 2. Figure 2 shows the frequency dependent opacity that was calculated by our code and that reported by Zeng *et al.* (2001).

The sharp absorption edge near 150 eV is attributed to the Al V ions, which is the most abundant species in such plasma conditions. As it can be seen in Figure 2, the results of our calculations are almost similar to those of reference (Zeng *et al.*, 2001). However, the results of our calculations show that the opacity values are slightly smaller than those of reference (Zeng *et al.*, 2001) especially in lower photon energy. Such discrepancy may be due to the atomic data that are used in two cases. In fact, the opacity calculation requires a large amount of atomic data, and the accuracy of the opacity strongly depends on the accuracy of the atomic data. The results were also compared to the calculated opacity which is available in TOPbase data (Magee *et al.*, 1995) (Fig. 3).

As the Figure 3 shows, the results of our calculations have similar trend to those in TOPbase and both results are fairly in good agreement. The absorption around 150 eV is mainly due to the *M*-shell transitions. The two main discrepancies including the number of bb transitions and the amplitude of the peaks are due to the fact that most of bb transitions (but not all) with larger oscillator strengths for the most abundant species in the plasma including Al V, Al VI, and Al IV ions were considered. Such results can be better fitted if one considers all of the bb absorption lines in the calculations. In addition, the consideration of more realistic line-broadening can produce an increase of the opacity. In this work, we just considered Doppler broadening in our calculations. Therefore, the results may be better fitted if we consider stark broadening. We will consider this issue in our future works.

In some practical applications such as energy transfer through hot dense matter, Rosseland and Planck mean opacities are used. The Rosseland and Planck mean opacities can be calculated by using relations Eqs. (10) and (11), respectively:

$$\kappa_{Rosseland} = \frac{\int_0^\infty \frac{\partial B_\nu}{\partial T} d\nu}{\int_0^\infty \frac{1}{\kappa_{ext.}} \frac{\partial B_\nu}{\partial T} d\nu}, \tag{10}$$

$$\kappa_{Planck} = \frac{\int_0^\infty \kappa_{abs} B_\nu d\nu}{\int_0^\infty B_\nu d\nu}. \tag{11}$$

https://doi.org/10.1017/S0263034613000244 Published online by Cambridge University Press

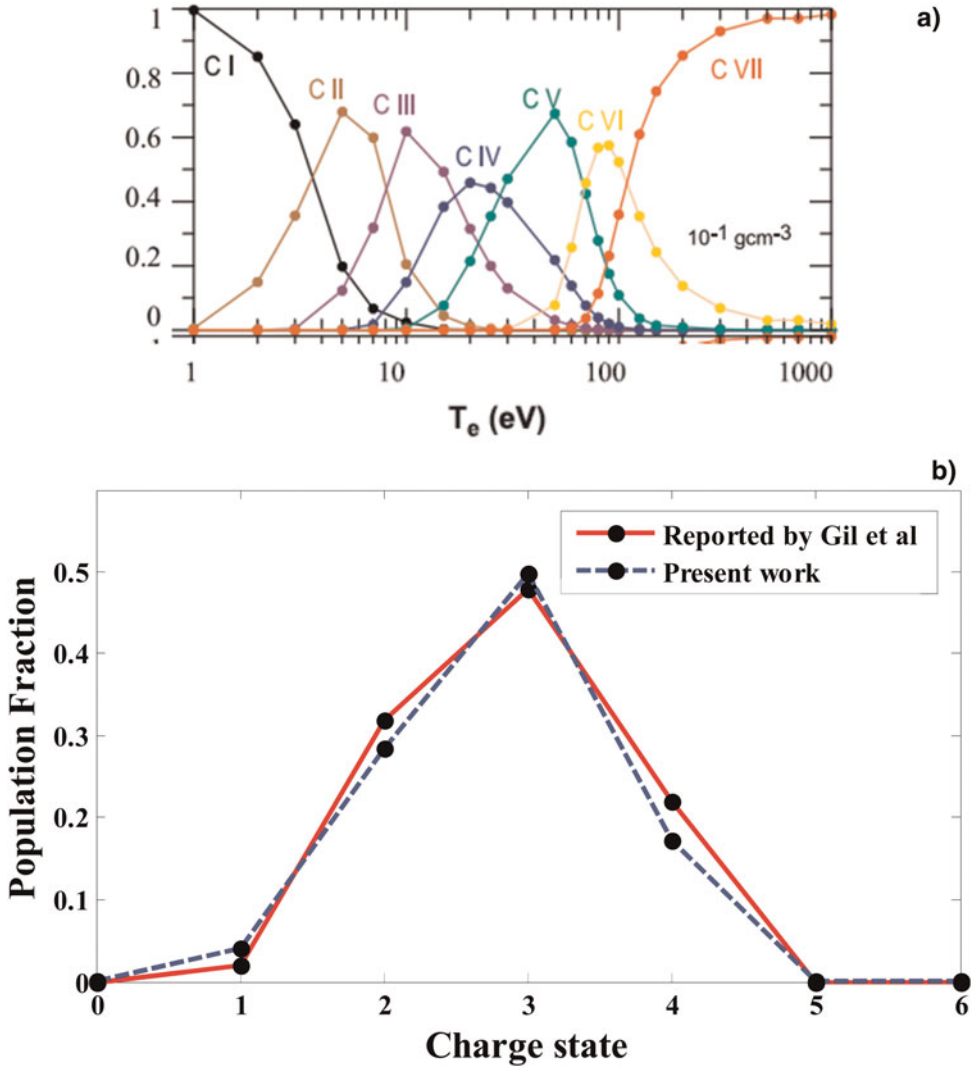

Fig. 4. (Color online) (**a**) Population fraction versus temperature for different carbon ions at density of 0.1 g/cm^{-3} (Gil *et al.*, 2013). (**b**) Population fraction versus the charge state for carbon plasma at temperature 20 eV, and density of 0.1 g/cm^{-3} (the results given by Gil *et al.*, 2013, and the present work).

Where $\kappa_{abs.}$ represents the plasma opacity due to absorption, $\kappa_{ext.}$ is the plasma opacity due to extinction (i.e., absorption and scattering), and B_ν is the Planck's black body function for a plasma at temperature T.

Table 3. *The ionization potential (IP) and the calculated ionization potential depression (IPD) for carbon plasma with the temperature of 20 eV and density of 0.1 g/cm^3*

Ions	IP (eV)	IPD (eV)
C I	11.26	4.75
C II	24.38	9.50
C III	47.89	14.25
C IV	64.49	19.01
C V	392.07	23.76
C VI	489.98	28.51

It may be useful to compare the Rosseland and Planck mean opacities with the frequency dependent opacities. For example, for aluminum plasma at temperature 20 eV, and density of 0.01 g/cm^{-3}, the Rosseland and Planck mean opacities were calculated by Zeng *et al.* (2006) and given as 4184 and 24891 cm^{2}g^{-1}, respectively.

For another example for validation of the code, we calculated the population fraction for carbon and compared the results with those of Gil *et al.* (2013). The results presented in Figure 4. In Figure 4a, the population fraction of different carbon ions (with density of 0.1 g/cm^3) versus temperature is presented. These results are obtained by Gil *et al.* (2013). For a specific temperature (such as 20 eV), one can easily extract the population fraction verses charge state out of Figure 4a. The results of such extraction for carbon plasma with temperature of 20 eV appear in Figure 4b.

Using our code, we also calculated the population fraction of carbon plasma (with temperature of 20 eV and density of

https://doi.org/10.1017/S0263034613000244 Published online by Cambridge University Press

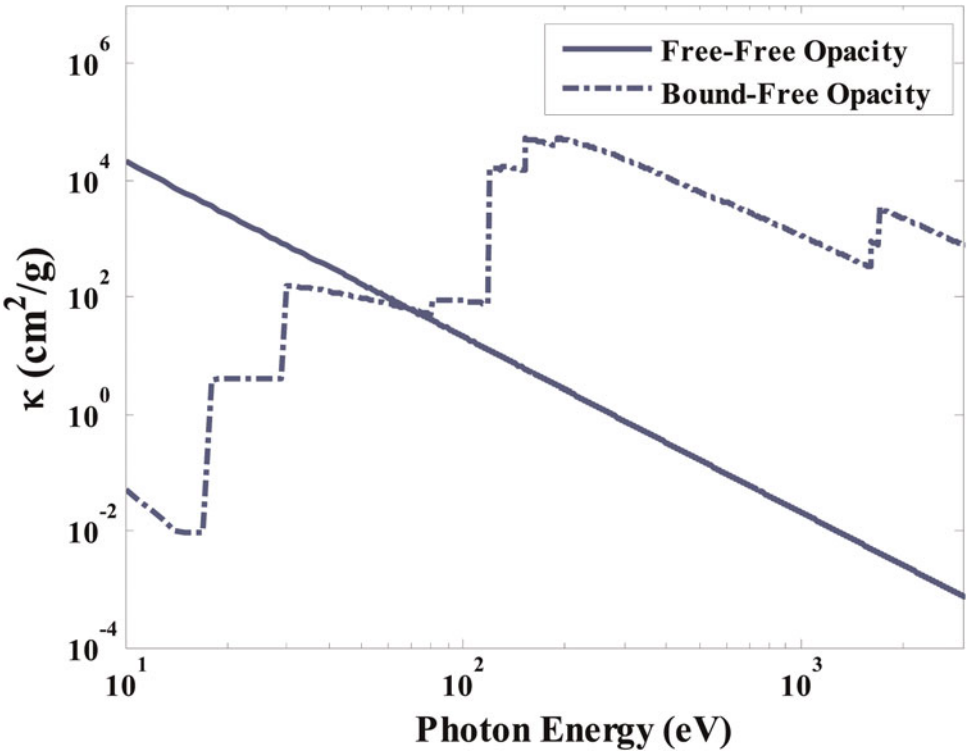

Fig. 5. (Color online) Free-free and bound-free absorption for aluminum plasma with the temperature of 20 eV and density of 0.01 g/cm^3.

0.1 g/cm^3) and presented the results in Figure 4b. Table 3 also gives the calculated IP and PD for carbon plasma ions with the temperature of 20 eV and density of 0.1 g/cm^3.

It can be seen that the population fraction increases for the carbon ions with the following form, i.e., C IV > C III > C V > C II. Figure 4 shows that there is good agreement between our results and those given by Gil *et al.* (2013).

RESULTS AND DISCUSSIONS

In this section, we have made a systematic study of the spectrally resolved opacities under different plasma conditions. Although the code is developed for all low-*Z* plasmas ($Z <$ 30), in this paper only carbon and aluminum plasmas were studied as two examples. In this section, we present some results for the opacity of two low-*Z* plasmas, i.e., carbon and aluminum plasmas. Carbon and aluminum plasmas have been of particular interests and were studied both experimentally and numerically (Jin *et al.*, 2008; Colgan *et al.*, 2006). The influences of plasma density and temperature were investigated on the frequency dependent opacity and the results were compared with those of cold matter.

Comparison between Free-Free Absorption and Bound-Free Absorption

For aluminum plasma with the temperature of 20 eV and density of 0.01 g/cm^3, individual opacities, i.e., ff and bf ones were presented in Figure 5 to give an estimation of their relative contributions to the opacity.

It can be seen in Figure 5 that the ff process is dominated for the lower energy photons but the bf contribution can exceed the ff absorption with increasing photon energy. According to this result, for photons with energies below about 50 eV, the major absorption mechanism is caused by ff absorption. However, with increasing the photon energy, bf absorption would play the major role for plasma with such density and temperature. As mentioned before the absorption edge near 150 eV is caused by the bf process of Al V ions that are the most abundant species in the plasma component at this density and temperature.

Density Dependence of Radiative Opacity

Figure 6a shows the opacity contributed by ff absorption and bf absorption for aluminum plasma versus photon energy at four different plasma densities 0.01, 0.1, 1, and 3 g/cm^{-3}. The temperature of the plasma in this figure was assumed to be 20 eV. The associated population fractions versus charge state for these aluminum plasmas are also presented in Figure 6b. Figure 6b shows that in aluminum plasma, the lower the density, the higher is the charge state for the population fraction peak. For example, for the plasma density of 0.01 g/cm^{-3}, the population fraction is maximum at charge state of about 5, while for the plasma density of 3 g/cm^{-3}, the population fraction peak shifts to charge state of about 2.8.

As the Figure 6a shows the plasma opacity increases with increasing the plasma density (within the photon energy

https://doi.org/10.1017/S0263034613000244 Published online by Cambridge University Press

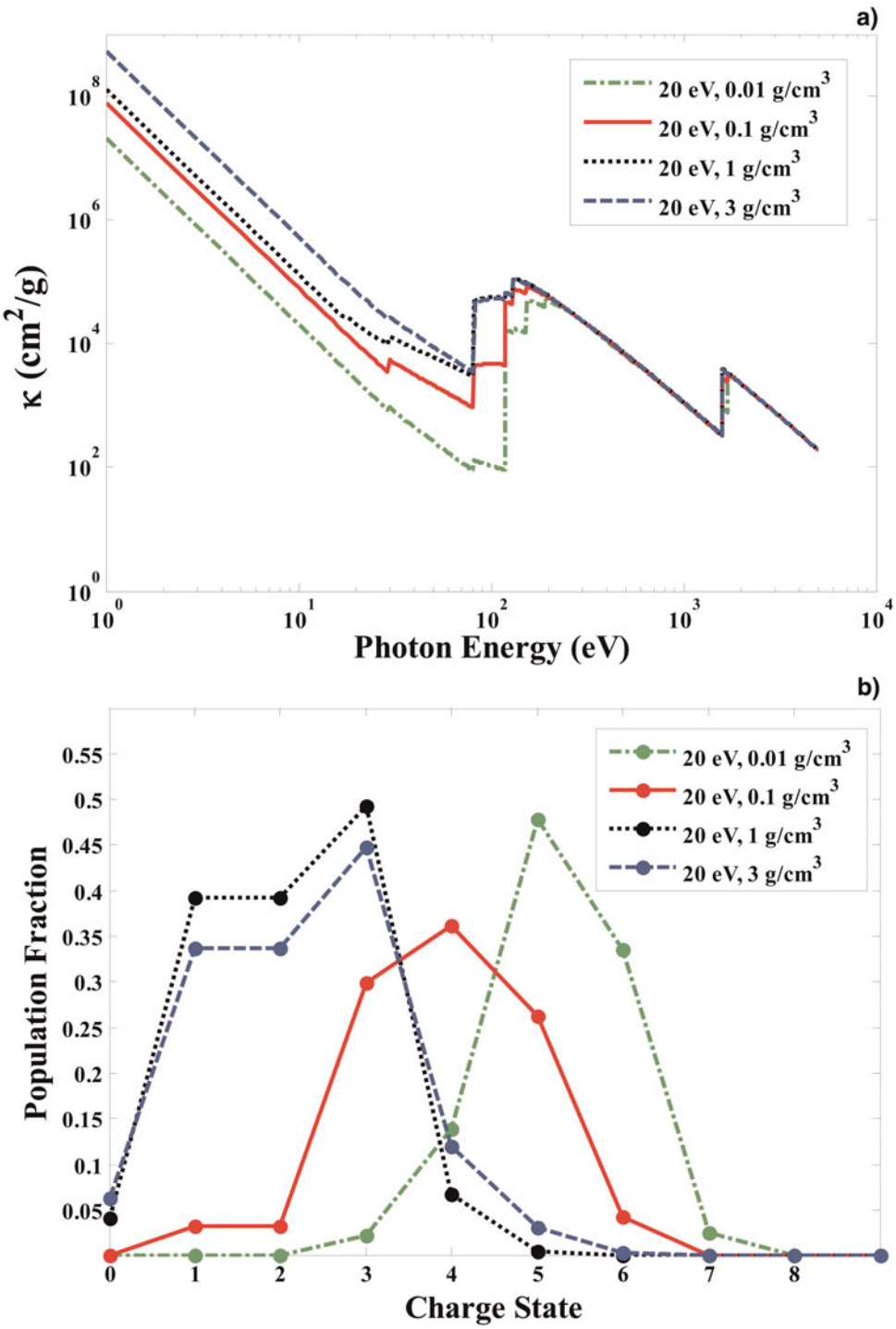

Fig. 6. (Color online) (**a**) Spectrally resolved radiative opacities for aluminum plasma at temperatures of 20 eV and densities of 0.01, 0.1, 1, and 3 g/cm^{-3}. (**b**) The population fraction versus charge state for aluminum plasmas at temperatures of 20 eV and densities of 0.01, 0.1, 1, and 3 g/cm^{-3}.

range up to about 240 eV) and then remains almost constant (with respect to plasma density). Such a result is due to the variation of populations. In fact, the abundance of plasma components' population is increased by increasing the plasma density; therefore, an increase in the total opacity is expected. This means that the lower density plasmas are more transparent for incident photons (photons with low energies).

As mentioned in the previous sections, the main absorption mechanism for low photon energy region is ff absorption. By increasing the plasma density, the population of electrons will also increase correspondingly. Consequently, the ff absorption

https://doi.org/10.1017/S0263034613000244 Published online by Cambridge University Press

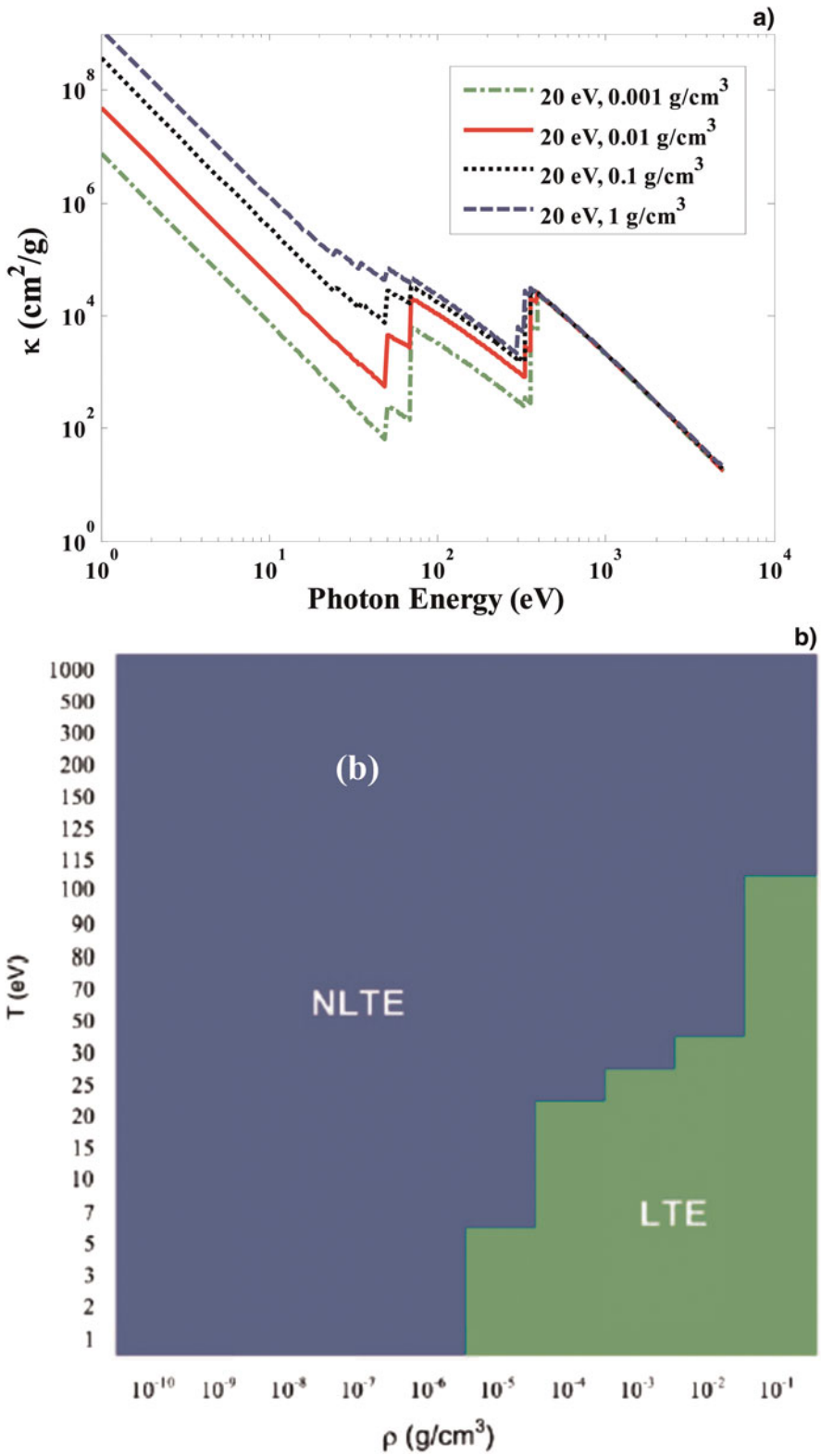

Fig. 7. (Color online) (**a**) Spectrally resolved radiative opacities for carbon plasma at a temperatures of 100 eV and density of 0.001, 0.01, 0.1, and 1 g/cm^{-3}. (**b**) The conditions for LTE and non-LTE carbon plasmas given by Gil *et al.* (2013).

is enhanced for higher plasma density. However, with increasing photon energy, the bf absorption is the dominant absorption mechanism in the plasma. Under such a plasma condition, the plasma components up to Al VII have more population and the absorption edges of these components shifts up to about 240 eV. Moreover, in plasma with a

https://doi.org/10.1017/S0263034613000244 Published online by Cambridge University Press

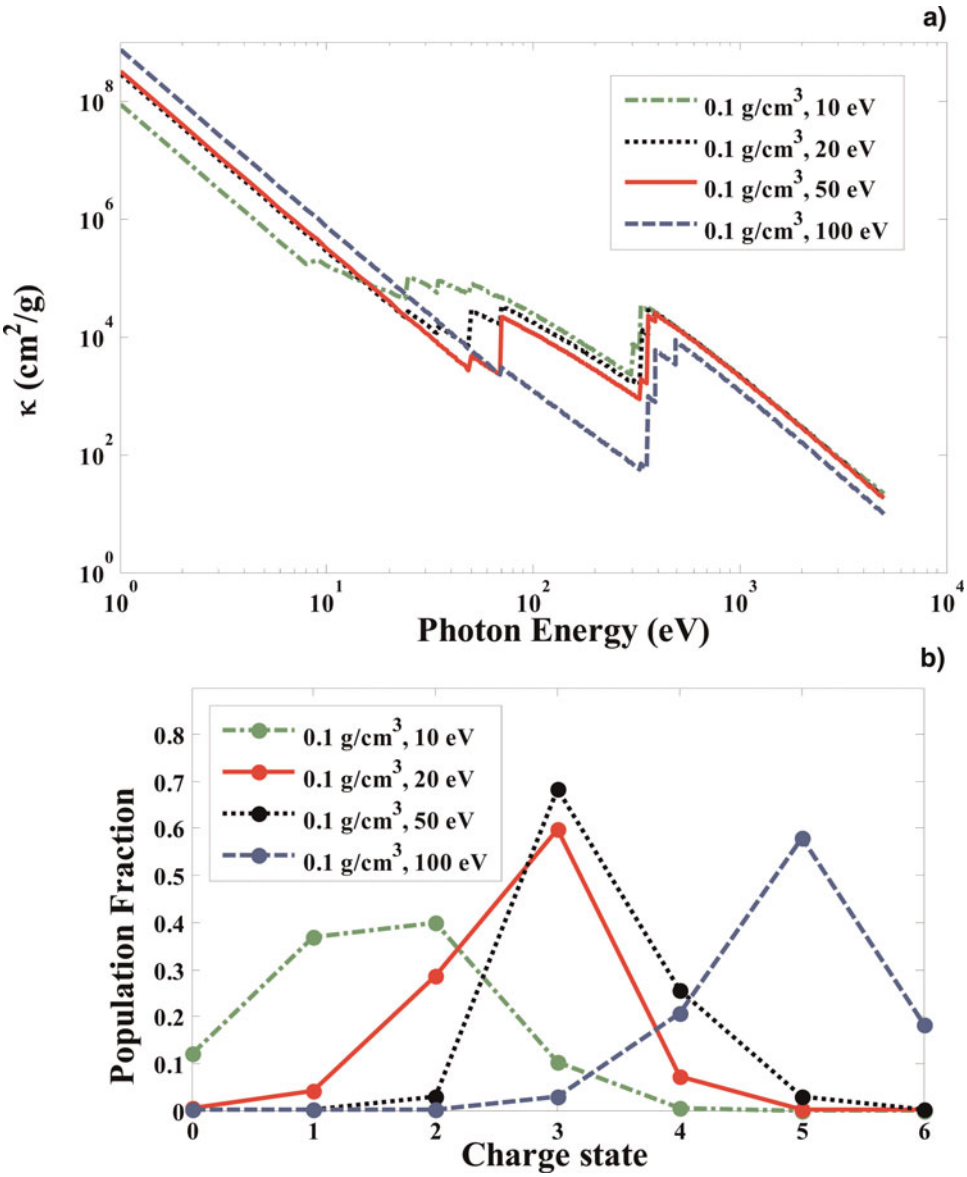

Fig. 8. (Color online) (**a**) Spectrally resolved radiative opacities for carbon plasmas at a density of 0.1 g/cm^{-3} and temperatures of 10, 20, 50, and 100 eV. (**b**) The population fraction versus charge state for carbon plasmas at a density of 0.1 g/cm^{-3} and temperatures of 10, 20, 50, and 100 eV.

temperature of 20 eV (which is low), the populations of plasma components for higher order ions are not varied significantly. Therefore, with increasing densities in aluminum plasma, it is not expected to have any significant change in total absorption for photons with energies higher than about 240 eV.

Figure 7a shows the opacity contributed by ff absorption and bf absorption for carbon plasma versus photon energy at temperature 20 eV, and different electron densities, i.e., 0.001, 0.01, 0.1, and 1 g/cm^{-3}.

In order to show that we are in LTE conditions, the results of LTE and non-LTE carbon plasmas (given by Gil *et al.*, 2013) are presented in Figure 7b. It must be noted that for colder carbon plasma (lower than 100 eV); the variations of opacity with different densities have a similar trend. However, we were interested to see the effect of plasma density for carbon plasma with temperature of about 20 eV in order to be able to compare the results with those of aluminum. Nevertheless, these results are partly similar to those of aluminum plasma. For example, the plasma opacity increases with increasing the plasma density (within the photon energy range up to about 500 eV). Such increment in opacity (for low photon energies) is due to enhancement of ff absorption. As explained for aluminum plasma, increasing the plasma density results in a rise of the population of electrons, which leads to enhancement of ff absorption. Therefore, the rise in opacity (versus plasma density) for photons with energies <500 eV, is mainly due to ff

https://doi.org/10.1017/S0263034613000244 Published online by Cambridge University Press

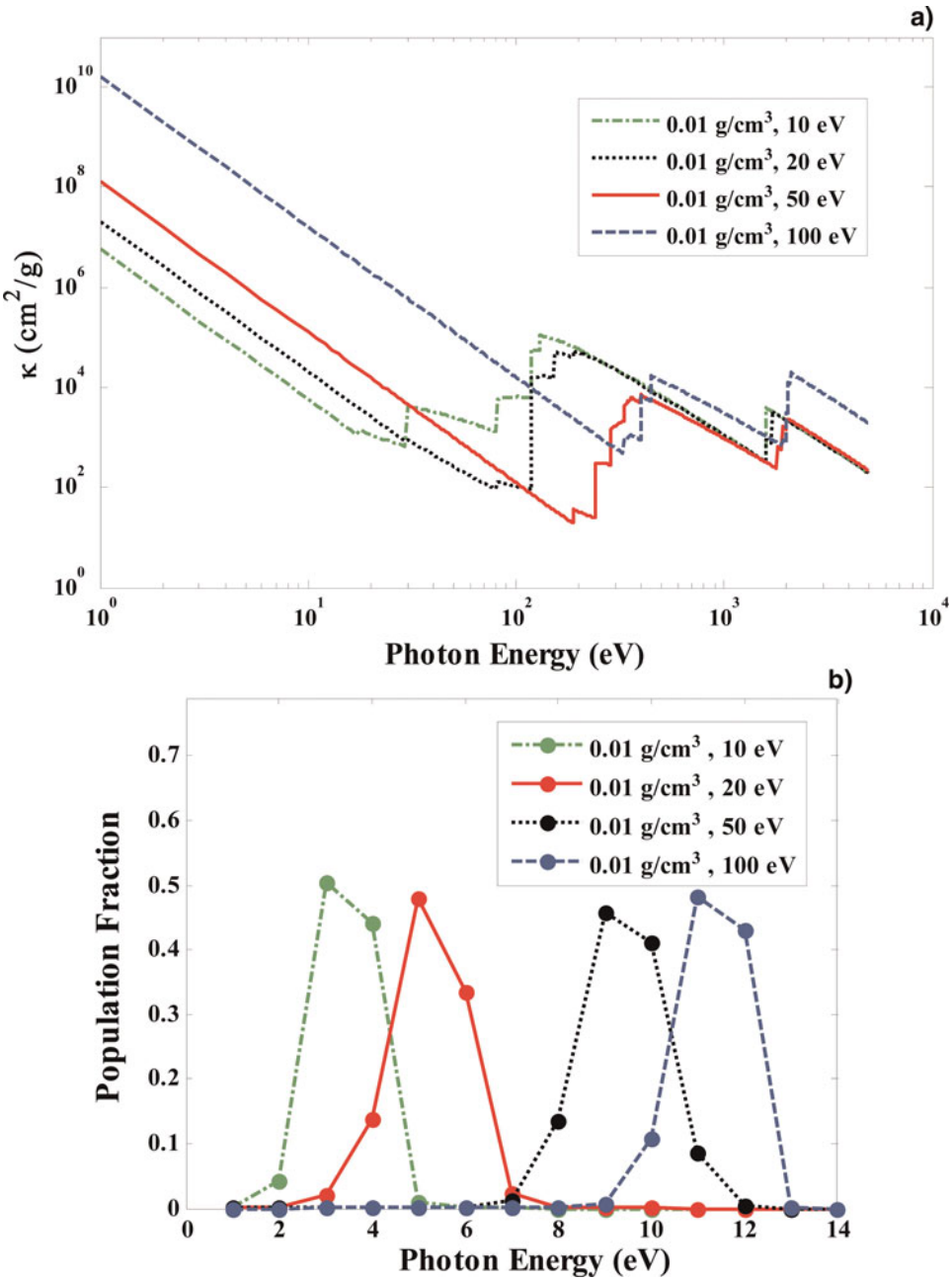

Fig. 9. (Color online) Spectrally resolved radiative opacities for aluminum plasmas at a density of 0.01 g/cm^{-3} and (**a**) temperatures of 10, 20, 50, 100 eV, and (**b**) the population fraction versus charge state for aluminum plasmas at a density of 0.01 g/cm^{-3} and temperatures of 10, 20, 50. and 100 eV.

absorption. As explained before, the fb absorption possesses a dominant effect in opacity for photons with higher energies. As the carbon plasma temperature rises (20 eV in our case), the populations of plasma components for higher order ions are varied significantly, which results in a growth of opacity when the plasma density increases. For example, Figure 7a shows a rise of one order of magnitude in opacity (for photon energies ranging from about 100 eV to 500 eV) when the plasma density changes from 0.001 g/cm^{-3} to 1 g/cm^{-3}.

Temperature Dependence of the Radiative Opacity

Figure 8a shows the carbon plasma opacity with respect to the photon energies for four different plasma temperatures 10, 20, 50, and 100 eV. In this figure, a density of 0.1 g/cm^{-3} was assumed for the plasma. The associated population fraction versus charge states is also presented in Figure 8b.

Figure 9a shows the opacity for aluminum plasma with respect to the photon energies for four different plasma

https://doi.org/10.1017/S0263034613000244 Published online by Cambridge University Press

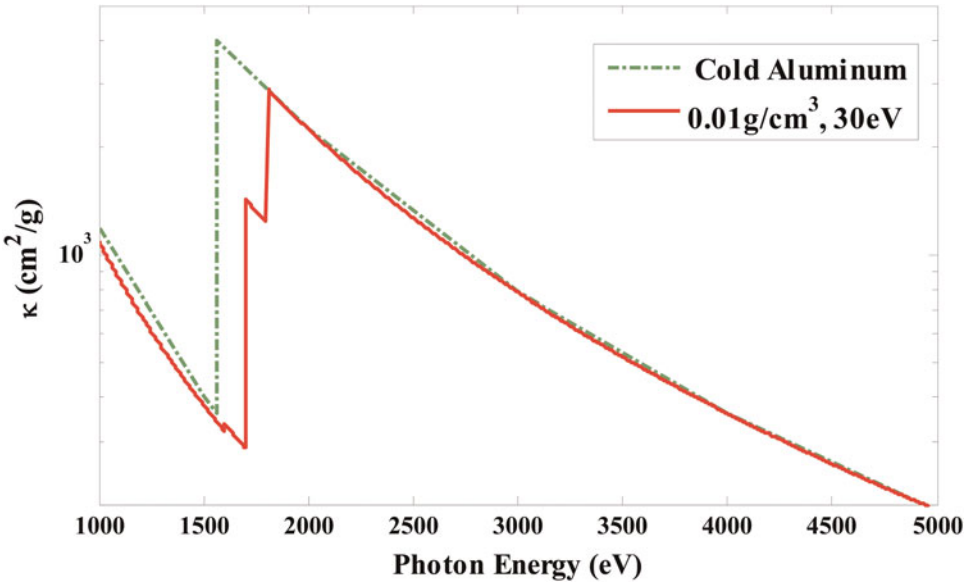

Fig. 10. (Color online) Spectrally resolved radiative opacities for cold aluminum and aluminum plasmas at a density of 0.01 g/cm^{-3} and temperatures of 30 eV.

temperatures 10, 20, 50, and 100 eV. In this figure, a density of 0.01 g/cm^{-3} was assumed for the plasma. The associated population fraction versus charge states for this plasma is also presented in Figure 9b. It must be noted that these temperatures and density were chosen to make sure that the calculations are performed for LTE conditions.

According to the results in Figures 8, and 9, the plasma opacity for low photon energies (almost photon energies <100 eV) rises with increasing temperature. However, such increment in opacity is insignificant for photon energies >100 eV. The behavior of the opacity with respect to temperature is mainly related to an ionization degree of the plasma. In fact, as the plasma temperature is increased, the average ionization degree of the plasma is increased, which in turn results in increasing the electron and ion density of the plasma. A similar explanation has been presented in reference (Rodríguez *et al.*, 2008).

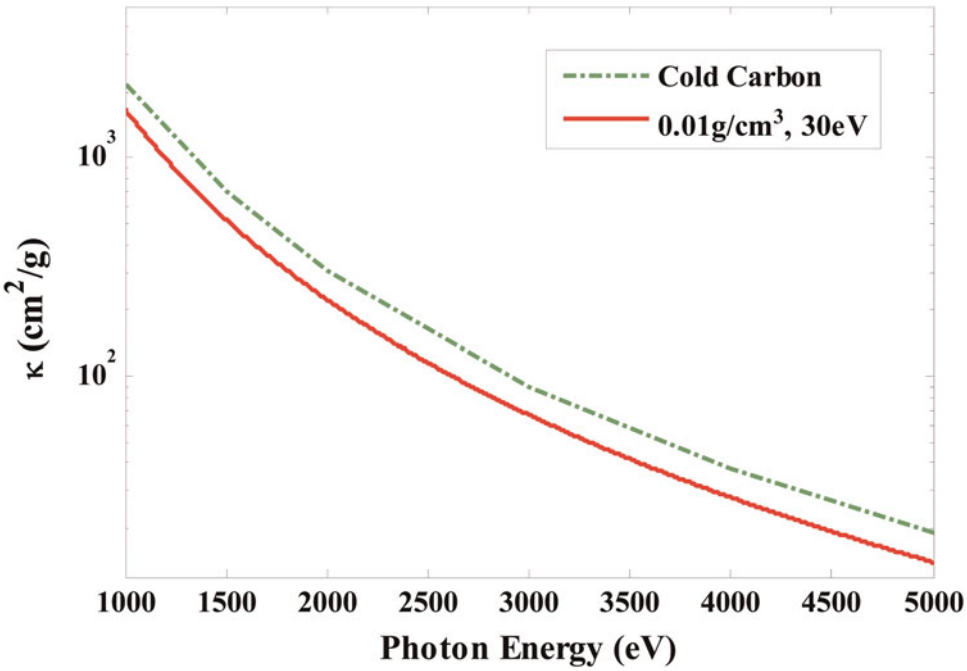

Fig. 11. (Color online) Spectrally resolved radiative opacities for cold carbon and carbon plasma at a density of 0.01 g/cm^{-3} and temperatures of 30 eV.

https://doi.org/10.1017/S0263034613000244 Published online by Cambridge University Press

Opacity Comparison between Cold Matter (Carbon and Aluminum), and Plasma (Carbon and Aluminum Plasmas)

Figure 10 shows the opacity contributed by ff absorption and bf absorption for cold aluminum and hot aluminum plasma versus photon energy at a density of 0.01 g/cm^{-3}. The opacity for cold aluminum was taken from NIST database which is mainly based on reference (Seltzer, 1993). The temperature of the plasma in this figure was assumed to be 30 eV. Similar calculations were performed for cold carbon and carbon plasma and almost similar results were obtained (Fig. 11).

As Figures 10 and 11 shows, with respect to cold matter, the opacity decreases for the matter in plasma state. For aluminum plasma, the absorption edge of the *K* shell is shifted to higher photon energy. The main reason for this trend of line shift is that the mean ionization degree increases with temperature. For instance, for aluminum at temperature of 30 eV and density of 0.01 g/cm^{-3}, the average ionization degree is 5.8. The corresponding maximum fraction of the aluminum ion at this condition is Al VII (about 50%). Any changes to the plasma condition may change the ion fractions and consequently the absorption lines shift to higher photon energy. However, for carbon plasma no absorption edge can be seen as there is no absorption edge within the photon energy ranges (i.e., 1000–5000 eV) in which the calculations were performed.

CONCLUSION

In this work, a computer code was developed for calculating the opacity of low-*Z* plasmas. The calculations are based on ff, bf, and bb transitions in LTE plasma. Atomic structures, transition levels, oscillator strengths, and others atomic data are provided for these calculations. The validation of the calculations was confirmed by comparing the calculation results of carbon and aluminum plasmas (at some specific conditions) with those of some others in literature such as TOPbase data and Zeng *et al.* (2000) results. The influences of plasma density and temperature on carbon and aluminum plasma opacities were investigated. From the results it was concluded that the opacity depends significantly on plasma characteristics, i.e., plasma temperature and density. Comparing the results with those of cold mater, it has been shown that the opacity may be changed significantly for the plasma state of the matter.

REFERENCES

Abdallah, Jr., J. & Clark, R.E.H. (1991). X-ray transmission calculations for an aluminum plasma. *J. Appl. Phys*. **69**, 23.

André, M., Babonneau, D., Bayer, C., Bernard, M., Bocher, J-L., Bruneau, J., Coudeville, A., Coutant, J., Dautray, R., Decoster, A., Decroisette, M., Desenne, D., Dufour, J-M., Garçonnet, J-P., Holstein, P-A., Jadaud, J-P., Jolas, A., Juraszek, D., Lachkar, J., Lascaux, P., Le Breton, J-P., Louis-Jacquet, M., Meyer, B., Mucchielli, F., Rousseaux, C., Schirmann, D., Schurtz, G., Véron, D. & Watteau, J-P. (1994). Progress in inertial confinement fusion physics at Centre d'Etudes de Limeil-Valenton. *Laser Part. Beams* **12**, 329–342.

Babonneaua, D., Bochera, J.L., Bayera, C., Decostera, A., Juraszeka, D., Perrinea, J.P. & Thiell, G. (1991). X-ray emission by the rear side of laser-irradiated gold targets, *Laser Part. Beams* **9**, 527–540.

Bailey, J.E., Rochau, G.A., Mancini, R.C., Iglesias, C.A., Mac Farlane, J.J., Golovkin, I.E., Blancard, C., Cosse, Ph, & Faussurier, G. (2009). Experimental investigation of opacity models for stellar interior, inertial fusion, and high energy density plasmas, *Phys. Plasmas* **16**, 1–16.

Bar-Shalom, A., Oreg, J., Goldstein, W.H., Shvarts, D. & Zigler, A. (1989). Super-transition-arrays: A model for the spectral analysis of hot, dense plasma. *Phys. Rev. A* **40**, 3183.

Bastiani, S., Giulietti, D., Giulietti, A., Gizzi, L.A., Ceccotti, T. & Macchi, A. (1995). A study of laser plasmas as X-ray sources in the 1-10 keV spectral region. *Laser Part. Beams* **13**, 493–501.

Bauche, J. & Bauche-Arnoult, C. (1996). Recent progress in the global description of atomic transitions. *Phys. Scr*. **99**, 1–13.

Bauche-Arnoult, C., Bauche, J. & Klapisch, M. (1978). Mean wavelength and spectral width of transition arrays in x-uv atomic spectra. *J. Opt. Soc. Am*. **68**, 1136.

Colgan, J., Fontesb, C.J. & Abdallah, Jr. J. (2006). Collisional-radiative studies of carbon plasmas. *Hi. Ener. Density Phys*. **2**, 90–96.

Cowan, R.D. (1981). *Theory of Atomic Spectra*. Berkeley: University of California Press,

Eliezer, S. (2002). *The Interaction of High-Power Lasers with Plasmas*. Philadelphia: IOP Publishing.

Faussurier, G., Wilson, B.G. & Chen, M.H. (2001). Generalization of super-transition-array methods to hot dense plasmas by using optimum independent particle reference systems. *Phys. Rev. E* **65**, 016403/1–5.

Gauthier, J.C., Amiranoff, F., Chenais-popovics, C., Jamelot, G., Koenig, M., Labaune, C., Leboucher-Dalimier, E., Sauteret, C. & Migus, A. (1999). LULI activities in the field of high-power laser–matter interaction. *Laser Part. Beams* **17**, 195–208.

Gil, J.M., Rodriguez, R., Martel, P., Florido, R., Rubiano, J.G., Mendoza, M.A. & Minguez, E. (2013). Analysis of the influence of the plasma thermodynamic regime in the spectrally resolved and mean radiative opacity calculations of carbon plasmas in a wide range of density and temperature. *J. Quant. Spectrosc. & Rad.e Trans*. **114**, 136–150.

Godwal, B.K., Sikka, S.K. & Kaushik, T.C. (1997). Equation of state in laser shock simulations. *Laser Part. Beams* **15**, 353–365.

Green, J.M. (1964). The statistical mechanics of the interdependent electrons in the screening constant model of the many-electron-atom. *J. Quant. Spectrosc. Radiat. Trans*. **4**, 639.

Gupta, N.K. & Godwal, B.K. (2001). Effects of various parameters on numerical simulations of inertial confinement fusion hohlraum and radiation hydrodynamics. *Laser Part. Beams* **19**, 259–265.

Gupta, N.K. & Godwal, B.K. (2002). Effects of non-local thermodynamic equilibrium conditions on numerical simulations of inertial confinement fusion plasmas. *Pramana J. Phys*. **59**, 33–51.

Gupta, N.K. & Kumar, V. (1995). Angular dependence of M and N band radiation and the effect of angular anisotropy on the total conversion efficiency of X rays emitted from a laser irradiated gold foil. *Laser Part. Beams* **13**, 389–402.

Heading, D.J., Wark, J.S., Bennett, G.R. & Lee, R.W. (1995). Simulations of spectra from dense aluminum plasmas. *J. Quant. Spectros. Rad. Trans*. **54**, 167–180.

Hutchinson, Ian H. (2002). *Principles of Plasma Diagnostics*. New York: Cambridge University Press.

Iglesias, C.A. & Rogers, F.J. (1996). Update OPAL opacities. *Astrophys. J*. **464**, 943.

Iglesias, C.A., Nash, J.K., Chen, M.H. & Rogers, F.J. (1994). Estimating plasma temperatures from transmission spectra, *J. Quant. Spectrosc. Radiat. Trans*. **51**, 125.

Jiao-Long, Z., Feng-Tao, J., Gang, J. & Jian-Min, Y. (2003). Temperature diagnostics for iron plasmas by means of transmission spectrum obtained by accurate atomic data, *Chin. Phys. Lett*. **20**, 862–864.

Jin, F., Zeng, J. & Yuan, J. (2008). Detailed diagnostics of a laser produced aluminum plasma by the Kalpha satellites. *J. Quant. Spectrosc. Radiat. Trans*. **109**, 2707–2714.

Kauffman, R.L., Suter, L.J., Darrow, C.B., Kilkenny, J.D., Kornblum, H.N., Montgomery, D.S., Phillion, D.W., Rosen, M.D., Theissen, A.R., Wallace, R.J. & Ze, F. (1994). High temperatures in inertial confinement fusion radiation cavities heated with 0.35 μm light. *Phys. Rev. Lett*. **73**, 2320–2323.

Magee, N.H., Abdallah, J., Clark, R.E.H., Cohen, J.S., Collins, L.A. & Csanak, G. (1995). Atomic structure calculations and new Los Alamos astrophysical opacities. *Astronomical Society of the Pacific Conference Series* **78**, 51–55.

Mahdieh, M.H. & Hosseinzadeh, S. (2010). Calculation of the radiative opacity for some low Z plasmas produced by high power pulsed lasers. *SPIE* **7751**, xxx.

Martin, W.C. & Zalubas, R. (1979). Energy levels of aluminum, Al I through Al XIII. *J. Phys. Chem. Ref. Data* **8**, 817.

Martin, W.C., Fuhr, J.R., Kelleher, D.E., Musgrove, A., Sugar, J., Wiese, W.L., Mohr, P.J. & Olsen, K. (2006). *NIST Atomic Spectra Database Version 2.0*. Gaithersburg, MD: National Institute of Standards and Technology.

Marzi, S., Giulietti, A., Giulietti, D., Gizzi, L.A. & Salvetti, A. (2000). A high brightness laser-plasma X-ray source at IFAM: characterization and applications. *Laser Part. Beams* **18**, 109–118.

Meister, C.-V., Imran, M. & Hoffmann, D.H.H. (2011). Relative energy level shifts of hydrogen-like carbon bound-states in dense matter. *Laser Part. Beams* **29**, 17–27.

Moore, C.E. (1970). Ionization potentials and ionization limits derived from the analysis of optical spectra. *Nat. Stand. Ref. Data Ser. Nat. Bur. Stand. (U.S.)* **34**, 22.

Nishimura, H., Endo, T., Shiraga, H., Kato, Y. & Nakai, S. (1993). X-ray emission from high-Z mixture plasmas generated with intense blue laser light, *Appl. Phys. Lett*. **62**, 1344–1346.

NIST database. http://physics.nist.gov/PhysRefData/XrayMassCoef/tab3.html.

Orlov, N.Yu., Denisov, O.B., Rosmej, O.N., Schäfer, D., Nisius, Th., Wilhein, Th., Zhidkov, N., Kunin, A., Suslov, N., Pinegin, A., Vatulin, V. & Zhao, Y. (2011). Theoretical and experimental studies of material radiative properties and their applications to laser and heavy ion inertial fusion. *Laser Part. Beams* **29**, 69–80.

Orlov, N.Yu., Guskov, S.Yu., Pikuz, S.A., Rozanov, V.B., Shelkovenko, T.A., Zmitrenko, N.V. & Hammer, D.A. (2007). Theoretical and experimental studies of the radiative properties of hot dense matter for optimizing soft X-ray sources. *Laser Part. Beams* **25**, 415–423.

Orzechowski, T.J., Rosen, M.D., Kornblum, H.N., Porter, J.L. & Suter, L.J. (1996). The Rosseland mean opacity of a mixture of gold and gadolinium at high temperatures, *Phys. Rev. Lett*. **77**, 3545–3548.

Ramis, R., Meyer-ter-Vehn, J. & Ramírez, J. (2009). MULTI2D – a computer code for two-dimensional radiation hydrodynamics. *Compu. Phys. Commun*. **180**, 977–994.

Rickert, A. & Meyer-Ter-Vehn, J. (1990). Frequency-dependent opacity calculations for high-Z plasma including l splitting. *Laser Part. Beams* **8**, 715–727.

Rodriguez, R., Florido, R, Gil, J.M., Rubiano, J.G., Martel, P., Mendoza, M.A., Suárez, D. & Mínguez, E. (2008). Detailed-level-accounting approach calculation of radiative properties of aluminum plasmas in a wide range of density and temperature, *J. Phys.: Confer. Ser*. **112**, 1–4.

Rodriguez, R., Florido, R., Gil, J.M., Rubiano, J.G., Martel, P. & Minguez, E. (2008). RAPCAL code: A flexible package to compute radiative properties for optically thin and thick low and high-Z plasmas in a wide range of density and temperature. *Laser Part. Beams* **26**, 433–448.

Rogers, F.J. & Iglesias, C.A. (1992). Radiative atomic Rosseland mean opacity tables. *Astrophys. J. Supp*. **79**, 507–568.

Rogers, F.J. & Iglesias, C.A. (1994). Astrophysical opacity. *Sci*. **263**, 50–55.

Rose, S.J. (1992). Calculations of the radiative opacity of laser-produced plasmas. *J. Phys. B: At. Mol. Opt. Phys*. **25**, 1667–1681.

Rose, S.J. (1991). High power laser produced plasma and astrophysics. *Laser Part. Beams* **9**, 869–879.

Rossall, A.K., Gartside, L.M.R., Chaurasia, S., Tripathi, S., Munda, D.S., Gupta, N.K., Dhareshwar, L.J., Gaffney, J., Rose, S.J. & Tallents, G.J. (2010). X-ray back-lighter characterization for iron opacity measurements using laser-produced aluminum K-alpha emission. *J. Phys. B: At. Mol. Opt. Phys*. **43**, 155403.

Rozsnyai, B.F. (1997). Collisional-radiative average-atom model for hot plasmas. *Phys. Rev. E* **55**, 7507–7521.

Rozsnyai, B.F. (2010). Hot plasma opacities in the presence or absence of local thermodynamic equilibrium. *Hi. Ener. Density Phys*. **6**, 345–355.

Seltzer, S.M. (1993). Calculation of photon mass energy-transfer and mass energy-absorption coefficients. *Rad. Res*. **136**, 147–170.

Verner, D.A., Ferland, G.J., Korista, K.T. & Yakovlev, D.G. (1996). Atomic data for astrophysics. II. New analytic fits for photo-ionization cross sections of atoms and ions. *Astrophys. J*. **465**, 487–498.

Winhart, G., Eidmann, K., Iglesias, C.A. & Bar-Shalom, A. (1996). Measurements of extreme UV opacities in hot dense Al, Fe, and Ho. *Phys. Rev*. **53**, R1332–R1335.

Yongqiang, L., Jianhua, W., Yong, H. & Jianmin, Y. (2009), Radiative opacities of hot and solid-dense aluminum plasmas using a detailed level accounting model. *J. Phys. B: At. Mol. Opt. Phys*. **42**, 1–11.

Zastrau, U., Burian, T., Chalupsky, J., Döppner, T., Dzelzainis, T.W.J., Fäustlin, R.R., Fortmann, C., Galtier, E., Glenzer, S.H., Gregori, G., Juha, L., Lee, H.J., Lee, R.W., Lewis, C.L.S., Medvedev, N., Nagler, B., Nelson, A.J., Riley, D., Rosmej, F.B., Toleikis, S., Tschentscher, T., Uschmann, I., Vinko, S.M., Wark, J.S., Whitcher, T. & Förster, E. (2012). XUV spectroscopic characterization of warm dense aluminum plasmas generated by the free-electron-laser FLASH. *Laser Part. Beams* **30**, 45–56.

Zel'dovich, Ya.B. & Raizer, Yu.P. (1966). *Physics of shock waves and High-Temperature Hydrodynamics Phenomena*. New York: Academic.

Zeng, J.L., Jin, F.T., Yuan, J.M., Lu, Q.S. & Sun, Y.S. (2000). Detailed-term-accounting-approximation simulation of x-ray transmission through laser-produced Al plasmas. *Phys. Rev. E* **62**, 7251.

Zeng, J., Jin, F. & Yuan, J. (2006). Radiative opacity of plasmas studied by detailed term (level) accounting approaches. *Frontiers Phys. China* **1**, 468–489.

Zeng, J., Yuan, J. & Lu, Q. (2001). Detailed-term-accounting-approximation calculations of the radiative opacity of laser-produced Al plasmas. *Phys. Rev. E* **64**, 066412/1–9.

Zhang, J., Key, M.H., Norreys, P.A., Danson, C., Neely, D., Rose, S.J., Walsh, F., Tallents, G.J., Dwivedi, L., Holden, M., Holden, P.B., Pert, G.J., Ramsden, S.A., Lewis, C.L.S., Macphee, A.G. & You, Y.L. (1996). Characteristics of rapidly recombining plasmas suitable for high-gain X-ray laser action. *Laser Part. Beams* **14**, 71–79.

https://doi.org/10.1017/S0263034613000244 Published online by Cambridge University Press